Journal of
Materials Chemistry B

PAPER

Cite this: J. Mater. Chem. B, 2015, 3, 4074

Multicavity halloysite–amphiphilic cyclodextrin hybrids for co-delivery of natural drugs into thyroid cancer cells†

M. Massaro,[a] S. Piana,[a] C. G. Colletti,[a] R. Noto,[a] S. Riela,*[a] C. Baiamonte,[b] C. Giordano,[b] G. Pizzolanti,[b] G. Cavallaro,[c] S. Milioto[c] and G. Lazzara*[c]

Received 28th March 2015,
Accepted 15th April 2015

DOI: 10.1039/c5tb00564g

www.rsc.org/MaterialsB

Multicavity halloysite nanotube materials were employed as simultaneous carriers for two different natural drugs, silibinin and quercetin, at 6.1% and 2.2% drug loadings, respectively. The materials were obtained by grafting functionalized amphiphilic cyclodextrin onto the HNT external surface. The new materials were characterized by FT-IR spectroscopy, SEM, thermogravimetry, turbidimetry, dynamic light scattering and ζ-potential techniques. The interaction of the two molecules with the carrier was studied by HPLC measurements and fluorescence spectroscopy, respectively. The release of the drugs from HNT–amphiphilic cyclodextrin, at two different pH values, was also investigated by means of UV-vis spectroscopy. Biological assays showed that the new complex exhibits anti-proliferative activity against human anaplastic thyroid cancer cell lines 8505C. Furthermore, fluorescence microscopy was used to evaluate whether the carrier was uptaken into 8505C thyroid cancer cell lines. The successful results revealed that the synthesized multicavity system is a material of suitable size to transport drugs into living cells.

Introduction

In recent years, there has been increasing interest in both life and materials science to use nanocontainers as carriers for the encapsulation and delivery of drug molecules.

Halloysite nanotubes (HNTs) are a biocompatible aluminosilicate clay, with a hollow tubular structure consisting of silica on the outer surface and alumina at the innermost surface.[1] HNTs and functionalized-HNTs (f-HNTs) are capable of entrapping a variety of active agents within the inner lumen as well as at the external surface, followed by their retention and slow release.[2] Due to their appealing characteristics, various exciting applications have been proposed for these nanomaterials. For instance, biomedical applications of HNTs include their use as gene delivery systems, cancer cell isolation, stem cell isolation, ultrasound contrast agents, bone implants, teeth fillers, cosmetics and controlled drug delivery.[3–8]

Cyclodextrins (CDs) are very promising materials in several fields. It is known that these macrocyclic compounds form inclusion complexes with small- and medium-sized organic molecules and the complexation reactions that are involved are highly important in drug delivery systems.[9] Furthermore, it was demonstrated that the use of amphiphilic cyclodextrins in drug delivery applications allows the increase of the range of potential drugs that can be encapsulated in the CD cavity.[10]

Recently we reported the first example of a new drug delivery system based on HNTs covalently linked to modified-cyclodextrin units employed as carriers for polyphenolic compounds like curcumin.[11]

Polyphenolic compounds, like flavonoids, that are ubiquitously distributed in plants have attracted considerable interest due to their wide variety of biochemical and pharmacological properties.[12,13] Unfortunately, their concentration in the blood circulation is likely to be low because they are sparingly soluble in water and chemically unstable in physiological medium.[14–16]

In order to protect these bioactive compounds against degradation factors and to enhance the bioavailability, various encapsulation and complexation methods are used.

In the present paper, we describe the synthesis and the characterization of a novel hybrid based on HNTs covalently linked to amphiphilic-cyclodextrin units. The advantages of multifunctional nanocarriers with the presence of two cavities

[a] Dipartimento STEBICEF, Sez. Chimica, Università degli Studi di Palermo, Viale delle Scienze, Parco d'Orleans II, Ed. 17, 90128 Palermo, Italy. E-mail: serena.riela@unipa.it; Fax: +39-091596825; Tel: +39-09123897546
[b] Dipartimento Biomedico di Medicina Interna e Specialistica, Sez. Endocrinologia, Diabetologia, Metabolismo, Università degli Studi di Palermo, 90127 Palermo, Italy
[c] Dipartimento di Fisica e Chimica, Università degli Studi di Palermo, Viale delle Scienze, Parco d'Orleans II, Ed. 17, 90128 Palermo, Italy. E-mail: giuseppe.lazzara@unipa.it

† Electronic supplementary information (ESI) available: FT-IR spectra, TGA details and details about p-HNT/silibinin and p-HNT/quercetin complexes. See DOI: 10.1039/c5tb00564g

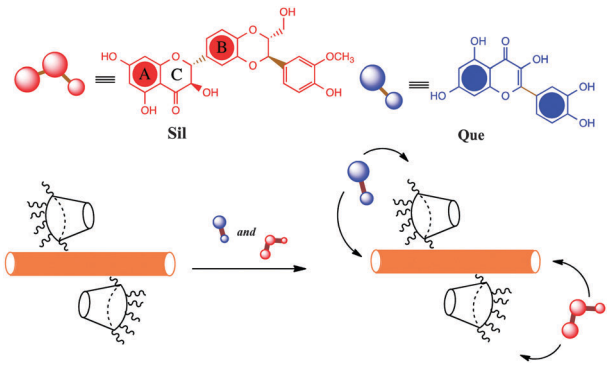

Fig. 1 Halloysite nanotube–amphiphilic cyclodextrin drug carrier.

offers the remarkable possibility for a simultaneous encapsulation of one or more drug molecules with different physico-chemical properties, followed by a different path release in agreement with the cavity that interacts with the drugs. Therefore, in order to employ the new system as a drug carrier we also studied its simultaneous interaction with two molecules, namely quercetin and silibinin, that possess different sizes and shapes (Fig. 1).

Indeed, co-delivery has attracted more and more attention because it is known that compared to conventional single-agent treatment, multi-agent therapy can promote synergism of different drugs, increase therapeutic target selectivity, and overcome drug resistance through distinct mechanisms of action.[17]

Results and discussion

Pristine halloysite was transformed as described into f-HNT-CD **1**,[10] and we used this material as a scaffold for the covalent linkage of alkyl thiols **2a–d** by thiol–ene reaction between vinyl groups on CDs and –SH groups on thiols (Scheme 1).

The reaction of **1** with alkyl thiols **2** was carried out by irradiation with UV light, from the Hg lamp, using toluene as solvent, in quartz vials at room temperature under an argon atmosphere. After 24 h, the compounds **3a–d** were obtained and analysed by TGA in order to evaluate the percentage of the loading, that was in the range among 0.6–2.9%.

It is interesting to note that, upon increasing the alkyl chain length of thiol (from **3a** to **3d**), we obtained materials with lower percentage loading (2.9 and 0.9%, respectively), as a consequence of enhanced steric hindrance on the HNT surface.

The grafting degrees provided an idea in terms of average positions substituted in the CD, namely it comes out that in

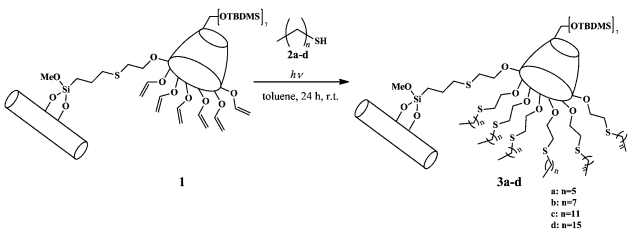

Scheme 1 Schematic representation for the linkage of alkyl thiols on compound **1**.

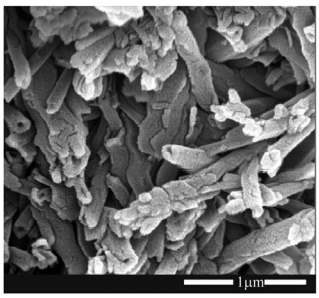

Fig. 2 SEM images of **3a**.

3a and **3b** the allyl groups have been fully substituted while **3c** and **3d** have an average of two substituted allyl groups.

The new materials were characterized by FT-IR spectroscopy, TGA and SEM measurements.

FT-IR investigation of **3a–d** shows that the vibrational bands of HNTs remain unaltered after the reactions. The frequency and assignments of each vibrational mode are based on previous reports on halloysite.[18]

Compared to **1** compounds **3a–d** exhibit an increase in the intensity of vibration bands for C–H stretching of methylene groups at around 2960 cm^{-1} and 2865 cm^{-1} (see ESI†).

The samples **3a–d** were investigated by means of TGA to determine the grafted amount of organic moieties. From a comparison with the thermogram of **1**, a further degradation and volatilization is observed accounting for the additional organic fraction. The grafting degrees were determined by comparing the residual masses at 900 °C of each **3a–d** and **1**. The obtained values are rather similar and range between 0.6 and 2.9 wt%.

Direct observation of the surface morphology of **3a–d** was accomplished by SEM. In all cases, the tubular shape of the nanoclay is not lost after grafting. Moreover, the lumen of the functionalized nanotubes appears empty, in agreement with the expected grafting at the external surface (Fig. 2).

Studies of the dispersions in aqueous medium

Turbidimetric analysis was performed to highlight the influence of functionalization on the dispersion stability of HNTs in aqueous media, which might be crucial for its application as a drug delivery system. Dispersions of **3a–c** showed a lower stability in water than **1**, according to the more hydrophobic surface functionalization in **3a–b** as compared to **1** (Fig. 3).

In contrast, dispersions of **3d** showed higher aqueous stability (Fig. 3) than **3a–b** and, surprisingly, even than **1**.

It is known[19] that the presence of the polymer and/or the surfactant at the nanoparticle surface may, generally, cause two different effects: (i) hydrophobic interactions that involve aggregation of material; (ii) steric repulsion or osmotic effects that involve an increase in repulsive interactions between nanoparticles and this generates stabilization of the dispersions.

The stability of the dispersions of compounds **3a–c** is controlled by hydrophobic interactions, while for **3d** a steric stabilization may occur.

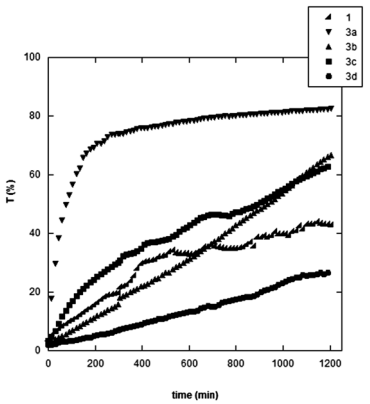

Fig. 3 Optical transmittance as a function of time for **1** and **3a–d** dispersions in water. The concentration is 0.1 wt% in all cases.

The diffusion coefficient of the nanoparticles in the solvent confirmed the results obtained by turbidimetric analysis. The diffusion coefficients of **3a–d** obtained by DLS experiments are collected in Table 1.

By comparing these results with the diffusion coefficient of **1** (11×10^{-13} m^2 s^{-1}) and HNTs in water (9.4×10^{-13} m^2 s^{-1})[20] it appears that **3a–b** form aggregates while **3c–d** show no aggregation.

With the aim of evidencing possible changes in the nanoparticle–nanoparticle electrostatic interactions, the ζ-potential in water was measured. All samples **3a–d** showed negative ζ-potential values (*ca.* −20 mV) close to that of HNTs (−19.5 mV). Therefore the electrostatic nanoparticle–nanoparticle repulsions are not altered by the surface functionalization, confirming that the aggregation of **3a–b** compounds is driven by van der Waals interaction and hydrophobic effects.

Interaction with silibinin and quercetin

With the aim of combining two or more drugs with synergistic therapeutic effects we verified the binding abilities of one of our new systems (**3a**) for two flavonoids, namely, silibinin (Sil) and quercetin (Que), chosen for their different affinities for the two cavities of the nanomaterial. We choose for the subsequent studies the **3a** compound in order to overcome problems of native CDs that limit their applications in pharmaceutical fields, for example to (i) enhance the interaction of CDs with biological membranes and (ii) modify or enhance interaction of CDs with hydrophobic drugs.[21] It should be noted that **3a** has the highest loading (2.9%) of amphiphilic cyclodextrins.

Experimental investigations performed by means of UV-vis and HPLC highlighted that silibinin did not interact with the cyclodextrin cavity, in contrast, it was encapsulated into the pristine HNT lumen as found by UV-vis spectroscopy and TGA (see ESI†).

Table 1 Diffusion coefficients for modified HNTs

Entry	Sample	D (10^{-13} m^2 s^{-1})
1	**3a**	5.57
2	**3b**	5.93
3	**3c**	9.53
4	**3d**	9.01

It is reported that native βCD is efficient in including quercetin.[22] In order to verify that the CD modification does not hinder the quercetin inclusion, supramolecular interactions with amphiphilic CDs (having the same substitution pattern of **3a**) have been studied. The formation of 1 : 2 quercetin/amph-CD complexes has been demonstrated by isothermal titration calorimetry (ITC) and UV-vis spectroscopy. The ITC data provided the equilibrium constant and the enthalpy change for the quercetin–amph-CD inclusion complex formation by assuming the equilibria:

$$\mathrm{CD} + \mathrm{Que} \overset{K_1}{\longleftrightarrow} \mathrm{CD-Que}$$

$$\mathrm{CD-Que} + \mathrm{CD} \overset{K_2}{\longleftrightarrow} \mathrm{CD-Que-CD}$$

and the procedure reported elsewhere.[23]

It was found $\beta = K_1 \times K_2 = (6.3 \pm 0.3) \times 10^5$ M^{-2} and $\Delta H_{ic} = -7.1 \pm 0.3$ kJ mol^{-1}, according to UV-vis results ($\beta = (9 \pm 2) \times 10^5$ M^{-2}) (see ESI† for details).

Furthermore fluorescence titration showed that this molecule also interacts with pristine HNTs (see ESI†). Recently, we have demonstrated that in the presence of HNT–cyclodextrin hybrids, curcumin, a biological molecule with a similar structure to quercetin, interacts preferentially with the cyclodextrin cavity.[11]

On the ground of this evidence we studied the interaction of **3a** with silibinin and quercetin by HPLC and fluorescence spectroscopy.

Reverse-phase HPLC equipped with a Diode-Array/UV detector offers the remarkable advantage of recording in real time the UV-vis spectrum of the chromatographic eluate (in the range of 200–600 nm), and therefore it allows the simultaneous monitoring of different species/analytes.

According to previous reports,[24] pure silibinin showed two peaks in the HPLC chromatogram, corresponding to the diasteroisomers silibinin A and B, with retention times (rt) of 2.67 and 3.53 minutes, respectively (eluent MeOH/H_2O 90 : 10 v/v, flow 1 mL min^{-1}). The most abundant component displayed two bands in the UV spectrum, the first one at 280 nm and the second one, less intense, at *ca.* 320 nm.

Pure quercetin showed one peak in the chromatogram at a rt of 3.38 min and it showed an UV spectrum with two bands at 250 and 370 nm.

No peaks were observed in the chromatogram related to **3a**, because this material showed no UV absorption.

Titration of fixed concentrations of silibinin and quercetin with **3a** (0–1.8 mg mL^{-1}) gave chromatograms (eluent MeOH/H_2O 90 : 10 v/v, flow 1 mL min^{-1}) which illustrated an unresolved broad peak at the rt range between 3.00 and 3.50 min, and presented a UV spectrum showing the same absorption maxima of silibinin. However, with the increasing amount of **3a** the UV spectrum displays a drastic change in the intensity of signal at 320 nm (Fig. 4).

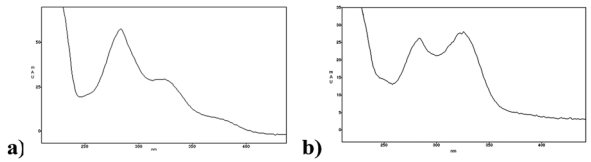

Fig. 4 UV-vis spectra of (a) silibinin and (b) **3a**–silibinin complex.

It is known that dihydroflavonols show two major absorption bands: band I (300–400 nm) and band II (240–280 nm).[25] Band I originates due to the light absorption of the A + C rings and corresponds to a π–π* transition; band II is due to the absorption of the B ring.

Therefore, because in our systems we have hypothesized that silibinin interacts with **3a** lumen, the different UV electronic absorption behaviour may be attributed to specific Sil–**3a** interactions in the form of hydrogen bonds and/or hydrophobic effects that involve phenolic OH groups of A rings. Similar results were obtained by Angelico *et al.* for the encapsulation of silibinin into liposomes.[26]

Being that silibinin in aqueous medium does not show emission, the interaction of quercetin and **3a**, in contrast, was studied by means of fluorescence spectroscopy.

The trend of fluorescence intensity of quercetin (1×10^{-4} M), recorded at 540 nm, with the increasing amount of **3a** (0–1.5 mg mL^{-1}) is reported in Fig. 5. This trend, related to the surnatant of the dispersions, is close to that obtained in the presence of crude amph-CD. Based on this finding and on the strong interaction evidenced by ITC and UV-vis between Que and amph-CD, one may hypothesize that quercetin interacts preferentially with the cyclodextrin cavity (Fig. 5). Similarly, curcumin, a hydrophobic drug, was selectively incapsulated into the CD instead of the hydrophilic HNT cavity.[11]

Loading silibinin into **3a** was carried out by vacuum cycling of a **3a** suspension in a saturated silibinin solution. This cycle was repeated several times in order to obtain the highest loading efficiency. After loading, the **3a**–Sil complex was washed in order to remove the free silibinin. **3a**–Sil was suspended again in water and then to this dispersion a saturated solution of quercetin was added. Subsequent investigations were conducted on the dry solid filtered from dispersion, washed with water and dried overnight at 60 °C.

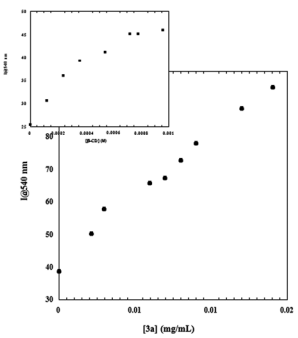

Fig. 5 Trend of the fluorescence intensity of quercetin, recorded at 540 nm, as a function of **3a** concentration (0–1.8 mg mL^{-1}) in the presence of a fixed amount of silibinin (1×10^{-4} M); the inset shows the fluorescence intensity of quercetin in the presence of increasing amounts of β-CD.

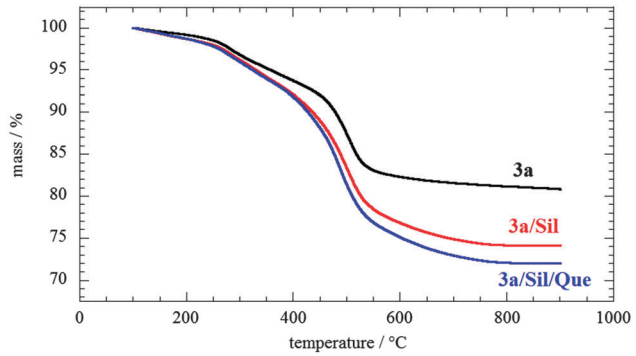

Fig. 6 Thermoanalytical curves for **3a** before and after drug loading.

The composite solids **3a**–Sil and **3a**–Sil–Que were characterized by TGA (Fig. 6). The thermoanalytical curves clearly show the successful loading of the drugs at each step. Given that both silibinin and quercetin degraded with a null residual at 900 °C, we calculated that compound **3a** is able to incorporate 6.1% of silibinin and 2.2% of quercetin. These results prove that the modified HNTs with a double cavity are efficient as nanocontainers for the co-delivery of two biological active molecules.

Kinetic release

In Fig. 7, an extended release profile of silibinin and quercetin from **3a**, in two different pH solutions, is shown.

The release of silibinin at pH 1 from compound **3a** reaches a plateau after 400 min, and an initial burst is observed within 200 min followed by a prolonged release.

The release profile obtained for quercetin showed a similar behavior to silibinin, but in this case a very low amount of molecule was released from the system (Fig. 7a). These results could be explained as follows. In acidic solution both **3a** and silibinin are positively charged; therefore, electrostatic repulsions may also accelerate the release of the drug from **3a**. In the case of quercetin it was reported that the retention efficiency of Que on β-CD is dependent on the pH, in particular it was larger in acidic solution than in neutral and basic media.[27] Therefore, the small amount of quercetin released from **3a** at pH 1 could be explained on the basis of strong interaction of the molecules and the CD cavity in acidic medium.

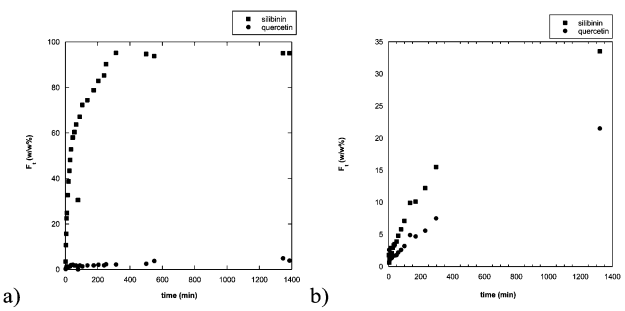

Fig. 7 Amount of silibinin and quercetin released from **3a** in (a) 0.1 M HCl solution; (b) pH 7.4 phosphate buffer.

In physiological medium, we observed that both molecules were released from the system; also in this case, quercetin was released in a smaller amount than silibinin. The different release in a neutral medium could be explained by taking into account that flavonoids are in their neutral form in a pH range between 4 and 6; therefore at physiological pH they could be partially dissociated and so more soluble in aqueous medium.

To better understand the release behaviour of silibinin and quercetin in different pH situations, the *in vitro* release data were fitted to various models to analyse the kinetics and the release mechanism of both molecules. The experimental data were analysed using the zero-order and first order equation, the double exponential model (DEM) and the Power law, to elucidate the release kinetics of silibinin at pH 1 and 7.4 and of quercetin at pH 7.4. It was found that the release mode of silibinin in acidic solution follows the double exponential model. According to the literature,[28] the DEM describes a mechanism consisting of two parallel reactions involving two spectroscopically distinguishable species. In our particular case, we observed the release of silibinin and the simultaneous, even if it is very low, release of quercetin ($k = 0.007 \pm 0.001$ min^{-1} and $k' = 0.064 \pm 0.006$ min^{-1}).

In physiological medium, release mode of silibinin and quercetin follows, in both cases, the first-order kinetics ($k = 0.0017 \pm 0.0001$ min^{-1} and 0.0007 ± 0.0001 min^{-1}, for silibinin and quercetin, respectively).

Desorption of silibinin and quercetin from **3a** can be described as the desorption of the molecules encapsulated into the HNT lumen and into the β-CD cavity, respectively.

In vitro cytotoxicity assay

We have tested the potential anti-proliferative *in vitro* activity of the **3a**–Sil–Que complex on an anaplastic thyroid cancer cell line: 8505C by means of MTS tests.

The survival rates of the tumor cells incubated with **3a** at each concentration were found in the range of 96–100%, indicating that they have no effect on the cell viability of the tumor cell lines under the concentration conditions investigated. Free quercetin and silibinin have no effect on cell viability, probably due to their rapid metabolism, systemic elimination and insolubility in physiological medium.

In contrast, the cell line showed a dose dependent cytotoxic profile when subjected to the treatment of **3a**–Sil–Que (see Fig. 8).

In particular, the concentration of **3a**–Sil–Que which caused 50% inhibition of cell growth was 27.6 ± 6.1 μM Compared to the free drugs, the HNT nanoparticles significantly improved the cellular cytotoxicity and exhibited the obviously synergistic effect by the co-delivery of two different anticancer drugs, silibinin and quercetin.

Cellular uptake of the drug into 3a

In the light of the potential application of **3a**–Sil–Que as the novel therapeutic treatment, several tests have been carried out *in vitro* to evaluate their uptake and localization into 8505C thyroid cancer cell lines. Indeed, for the internalization of nanoparticles by tumor cells it is essential to liberate therapeutic agents into the cytosol where most therapeutic agents accumulate and exhibit effect.

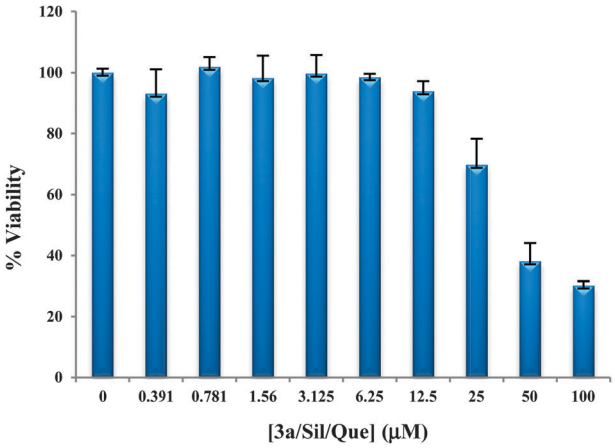

Fig. 8 MTS test for the cell viability of 8505C cells cultured for 72 h in the presence of **3a**–Sil–Que.

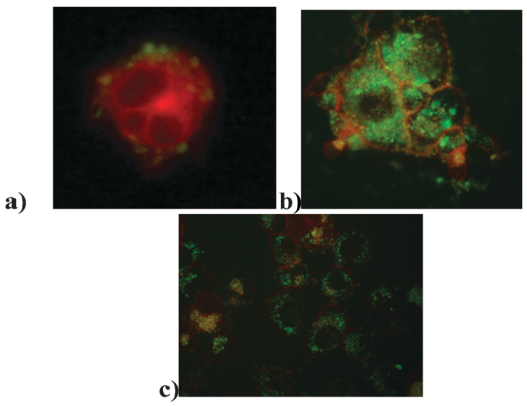

Fig. 9 Fluorescence microscopy images of the **3a** uptake by 8505C. 8505C cell membrane (red) with co-localised **3a** (green) outside nuclei at (a) 1 h and (b and c) 24 h.

For this purpose, we analyzed, by means of fluorescence microscopy, the interaction between cells and the carrier.

Fluorescence microscopy data revealed that **3a** showed a high propensity to cross cell membranes resulting in a massive cell uptake, as highlighted by the fluorescence emission localized in the cytoplasm. In particular, halloysite nanoparticles penetrate into the cells and concentrate around the cell nucleus from the observation of the silibinin fluorescence signal (green) within cells (Fig. 9). The results suggested that the **3a**–Sil–Que complexes could be effectively transported into living cells.

Experimental section

All needed reagents were used as purchased (Aldrich), without further purification.

Cyclodextrin functionalized HNTs were prepared according to the previous report.[11]

Heptakis-6-(*tert*-butyldimethylsilyl)-2-propaneoxy-2-hexanethio-β-cyclodextrin was synthesized as described below.

The chromatographic measurements were performed using a Shimadzu Class VP (Shimadzu, Japan) which consists of a pump (LC-10AD VP Shimadzu), an injection valve equipped with a 20 μL injection loop, an UV-vis Diode-Array (SPD-M10A VP) and an acquisition data software Class-VP. After optimization of chromatographic conditions, separation was carried out in a C_{18} column (Discovery Supelco, 25 cm × 4.6 mm, 5 μm). The mobile phase consisted of methanol/water 90 : 10 v/v, at room temperature, flow 1 mL min^{-1}.

An AESEM FEI QUANTA 200F microscope apparatus was used to study the morphology of the functionalized HNTs. Before each experiment, the sample was coated with gold under argon by means of an Edwards Sputter Coater S150A, in order to avoid charging under electron beam.

Thermogravimetric analyses were performed on a Q5000 IR apparatus (TA Instruments) under a nitrogen flow of 25 cm^3 min^{-1} for the sample and 10 cm^3 min^{-1} for the balance. The weight of each sample was *ca.* 10 mg. Measurements were carried out by heating the sample from rt up to 900 °C at a rate of 10 °C min^{-1}.

IR spectra (KBr) were recorded using an Agilent Technologies Cary 630 FT-IR spectrometer. Specimens for measurements were prepared by mixing 5 mg of the sample powder with 100 mg of KBr.

DLS measurements were performed at 22.0 ± 0.1 °C in a sealed cylindrical scattering cell at a scattering angle of 90°, by means of a Brookhaven Instrument apparatus composed of an BI-9000AT correlator and a He–Ne laser (75 mW) at a wavelength (λ) of 632.8 nm. The solvent was filtered through a 0.45 μm pore size Millipore filter. For all systems, the field-time autocorrelation functions were well described by a mono-exponential decay function, which provides the decay rate (Γ) of the single diffusive mode. For the translational motion, the collective diffusion coefficient at a given concentration is $D_t = \Gamma/q^2$ where q is the scattering vector given by $4\pi n\lambda^{-1}\sin(\theta/2)$, n is the water refractive index and θ is the scattering angle.

Turbidimetric and UV-vis measurements were performed using a Beckmann DU 650 spectrometer.

The ITC experiments were carried out at 298 K by means of a nano-ITC200 calorimeter (MicroCal). An amount of approximately 40 μL of quercetin solution (2 mmol dm^{-3}) was injected into the thermally equilibrated ITC cell (202 μL) filled with the CD solution (0.1 mmol dm^{-3}). The solvent was phosphate buffer (pH = 6.9)/MeOH 6 : 4. The heat effect was measured after each addition of 2 μL and corrected by dilution effects.

The dispersions were sonicated using an ultrasound bath VWR Ultrasonic Cleaner (power 200 W and frequency 75 MHz).

ζ-Potential measurements were performed by means of a ZETASIZER NANO ZS90 (Malvern Instruments).

Steady-state fluorescence spectra were acquired using a JASCO FP-777W spectrofluorimeter. Excitation and emission slits were 1.5 and 3 nm, respectively, the excitation wavelength was 372 nm and the emission interval was between 300 and 750 nm.

Synthesis of heptakis-6-(*tert*-butyldimethylsilyl)-2-propaneoxy-2-hexanethio-β-cyclodextrins

In a quartz test tube the heptakis-6-(*tert*-butyldimethylsilyl)-2-allyloxy-β-cyclodextrin[29] (100 mg, 46.2 mmol, 1 eq.) and hexanethiol (0.23 mL, 1.62 mmol, 35 eq.) were dissolved in distilled 95% toluene/MeOH (the concentration of CDs was 5 mM). A stream of Ar was bubbled through the solution for 15 min to thoroughly degas it. The test tube, maintained under an atmosphere of Ar, was placed in front of a Hg lamp (265 nm) and stirred for 20 h. Following removal of solvent, the residue was washed three times with hexane and purified by chromatography (SiO_2, from 100% hexane/EtOAc to 50% hexane/EtOAc) to afford the product as a white solid (yield 82%).

^{1}H NMR (DMSO, 300 K, 300 MHz) δ: 0.2 (42H, s), 0.88 (21H, t, J = 9.5 Hz), 0.98 (63H, s), 1.30 (28H, m), 1.42 (14H, m), 1.63 (14H, m), 1.90 (14H, m), 2.68 (14H, m), 2.79 (14H, m), 3.37 (14H, t, J = 7.4 Hz), 3.02 (7H, dd, J = 3.0 Hz, J = 9.5 Hz), 3.54 (14H, m), 3.59 (7H, bs), 3.79 (7H, m), 3.99 (14H, m), 4.94 (7H, d, J = 3.3 Hz).

^{13}C NMR (DMSO, 300 K, 75 MHz) δ: 4.9, 14.1, 22.7, 25.9, 28.2, 30.6, 30.8, 31.1, 33.2, 73.5, 62.5, 74.4, 74.9, 75.9, 79.7, 102.0.

Synthesis of compounds 3a–d

The appropriate thiol **2a–d** (1000 eq.) and modified HNT **1** (100 mg) were dissolved in anhydrous toluene. A stream of Ar was bubbled through the solution for 15 min to thoroughly degas it. The solution, maintained under an atmosphere of Ar, was placed in front of a Hg lamp and stirred for 24 h. Following removal of solvent, the precipitate was washed with CH_2Cl_2 and dried overnight at 80 °C under vacuum.

General procedure to obtain 3a/biological molecule dispersions

Various weighed amounts of p-HNT or **3a** (from 2 up to 14 mg) were dispersed by sonication for 5 minutes in H_2O, at an ultrasound power of 200 W and a temperature of 25 °C. 1 mL of appropriate biological molecule solution (1×10^{-4} M) in a mixture of pH 6.9 buffer/EtOH (6 : 4) was added to the p-HNT or **3a** dispersions. The final volume was 10 mL.

General procedure to obtain solid complexes

To a dispersion of **3a** in deionized water (5 mL), 1 mL of silibinin solution 10^{-2} M in ethanol was added. The suspension was sonicated for 5 min, at an ultrasound power of 200 W and at 25 °C and then was evacuated for 3 cycles. The suspension was left under stirring for 24 h at room temperature. After this time the powder was washed with water and then dried at 80 °C under vacuum. Afterwards the **3a**–silibinin solid complex was suspended again in deionized water (5 mL) and 1 mL of quercetin solution (10^{-2} M) in ethanol was, then, added. The suspension was stirred for 4 days at rt and then was filtered; the powder was washed with small amounts of water and then dried at 70 °C under vacuum overnight.

General procedure for spectrophotometric measurements

Measurement solutions were prepared by adding increasing volumes of the solution of heptakis-6-(*tert*-butyldimethylsilyl)-2-propaneoxy-2-hexanethio-β-cyclodextrins in phosphate buffer

(pH 6.9) (1.2×10^{-3} M) to 100 μL of the quercetin aqueous solution into a volumetric flask. In these solutions, the concentrations of the quercetin were constant and equal to 1×10^{-5} M while the concentration of the heptakis-6-(*tert*-butyldimethylsilyl)-2-propaneoxy-2-hexanethio-β-cyclodextrin increased from 1.2×10^{-4} M up to 1.08×10^{-3} M. The absorbance was recorded at 370 nm and spectroscopic data were fitted using the following equation (the non-linearized version of Benesi–Hildebrand treatment):

$$\mathrm{CD} + \mathrm{Que} \overset{K_1}{\longleftrightarrow} \mathrm{CD-Que}$$

$$\mathrm{CD-Que} + \mathrm{CD} \overset{K_2}{\longleftrightarrow} \mathrm{CD-Que-CD}$$

$$\Delta A = \frac{\Delta\varepsilon \cdot \beta \cdot \mathrm{Que} \cdot [\mathrm{CD}]^2}{1 + \beta \cdot [\mathrm{CD}]^2} \quad (1)$$

$$\beta = K_1 \cdot K_2$$

where $\Delta\varepsilon$ is the difference of the extinction molar coefficient of free and complexed quercetin, and Que and CD are the total concentration of the quercetin and the heptakis-6-(*tert*-butyldimethylsilyl)-2-propaneoxy-2-hexanethio-β-cyclodextrin, respectively.

Kinetic release

The release of quercetin and silibinin from the **3a**–Sil–Que complexes was done as follows: 25 mg of the sample were dispersed in 1 mL of dissolution medium and transferred into a dialysis membrane (Medicell International Ltd MWCO 12-14000 with a diameter of 21.5 mm). Subsequently the membrane was put in a round bottom flask containing 10 mL of the release medium at 37 °C and stirred.

Two different media (0.1 M HCl and phosphate buffer pH 7.4, respectively) were considered in order to evaluate the influence of pH on the release behavior of the drug.

At fixed time, 1 mL of the release medium has been withdrawn and analyzed by UV-vis (at 250 and 290 nm for quercetin and silibinin, respectively). To keep constant the volume of the release medium, 1 mL of fresh solution (0.1 M HCl, pH 7.4 buffer) has been used to replace the collected one.

The quercetin and silibinin concentrations in the solution were determined by UV-vis spectrophotometry using the Lambert–Beer law.

Total amounts of drug released (F_t) were calculated as follows:

$$F_t = V_\mathrm{m} C_t + \sum_{i=0}^{t-1} V_\mathrm{a} C_i \quad (2)$$

where V_m and C_t are the volume and the concentration of the drug at time t. V_a is the volume of the sample withdrawn and C_i is the drug concentration at time i ($i < t$).

Cell culture

8505c anaplastic thyroid cancer cells (ECAC Sigma-Aldrich, Milan, Italy) were grown in RPMI1640 (Sigma-Aldrich, Milan, Italy) supplemented with 10% FCS (Sigma-Aldrich, Milan, Italy), 2 mM L-glutamine and penicillin–streptomycin and incubated at 37 °C in 5% CO_2 and 100% humidity.

MTS assay

8505c cells were plated at 1500 cells per well in triplicate in a 96-well plate. After 24 h of incubation, **3a**–Sil–Que drug suspension was added ranging from 100 μM to 0.391 μM. After 72 h of incubation the plate was washed with sterile PBS, to avoid colour interference from the **3a**–Sil–Que compound. 20μL of the CellTiter 96 AQueous One Solution (Promega, Milan, Italy) was added, and the plate was incubated for 4 hours at 37 °C. The absorbance at 490 nm was recorded using a plate reader (Multiskan™ TC Microplate Photometer, Thermo SCIENTIFIC, Milan Italy). The results were expressed as % of viability with respect to the control cells that were not treated.

IC_{50} was calculated by Global Optimization using Simulated Annealing Software (GOSA-fit) and was found to be 27.6 ± 6.1 μM.

Fluorescence microscopy

8505c cells were seeded in a Nunc Lab-Tek Chamber Slide (Nunc, Italy) at a density of 300 000 cells per slide in RPMI culture medium and incubated under standard conditions. After 24 hours **3a** was added at 10 μM and incubated for 1 hours and 24 hours, respectively. Slides were then extensively washed with PBS-containing Ca and Mg and counterstained with Evans Blue in PBS at 0.005%. Slides were observed using a Zeiss Axiophot fluorescence microscope with a FITC filter equipped with a Nikon DS-Fi1 CCD-camera.

Conclusions

We have developed a new nanocarrier composed of biodegradable halloysite nanotube–amphiphilic cyclodextrins for the co-delivery of silibinin and quercetin as a potential combination therapy for the treatment of thyroid cancer.

Multicavity halloysite-nanotube materials were obtained by grafting amphiphilic cyclodextrin units onto the nanotube surface. The obtained materials were characterized by FT-IR spectroscopy, and TGA and SEM investigations.

In order to exploit their ability as drug carriers we, also, performed turbidimetric analysis in aqueous medium, which showed that, depending on the alkyl chain length of alkyl groups on cyclodextrins, the materials were like aggregates. These results were confirmed by DLS and ζ-potential investigations.

We studied the binding abilities of the systems with two biologically active molecules, namely quercetin and silibinin.

HPLC measurements and fluorescence spectroscopy highlighted that silibinin interacts preferentially with the HNT lumen, while quercetin does with the cyclodextrin cavity.

The kinetic release of the two molecules from the multicavity system was also carried out. In addition, TGA results showed that the new materials can load with efficiency the drugs and therefore, they are suitable nanocontainers for co-delivery of two drugs

that could have synergic effects in anticancer therapy as demonstrated by *in vitro* cytotoxicity assays.

Finally, the interaction between cells and the carrier, analyzed by fluorescence microscopy, revealed that the materials were uptaken into cells surrounding the nuclei. Therefore the multicavity systems could transport drugs into living cells.

Acknowledgements

This work was financially supported by the University of Palermo, PRIN 2010-2011 (prot. 2010329WPF) and FIRB 2012 (prot. RBFR12ETL5).

Notes and references

1 Y. Lvov and E. Abdullayev, *Prog. Polym. Sci.*, 2013, **38**, 1690.
2 (*a*) S. Riela, M. Massaro, C. G. Colletti, A. Bommarito, C. Giordano, S. Milioto, R. Noto, P. Poma and G. Lazzara, *Int. J. Pharm.*, 2014, **475**, 613; (*b*) M. Massaro, C. G. Colletti, R. Noto, S. Riela, P. Poma, S. Guernelli, F. Parisi, S. Milioto and G. Lazzara, *Int. J. Pharm.*, 2015, **478**, 476; (*c*) E. Joussein, S. Petit, J. Churchman, B. Theng, D. Righi and B. Delvaux, *Clay Miner.*, 2005, **40**, 383.
3 V. Vergaro, Y. M. Lvov and S. Leporatti, *Macromol. Biosci.*, 2012, **12**, 1265.
4 H. Kelly, P. Deasy, E. Ziaka and N. Claffey, *Int. J. Pharm.*, 2004, **274**, 167.
5 D. Kommireddy, I. Ichinose, Y. M. Lvov and D. Mills, *J. Biomed. Nanotechnol.*, 2005, **1**, 286.
6 Y. F. Shi, Z. Tian, Y. Zhang, H. B. Shen and N. Q. Jia, *Nanoscale Res. Lett.*, 2011, **6**, 608.
7 A. D. Hughes, J. Mattinson, J. D. Powderly, B. T. Greene and M. R. King, *J. Visualized Exp.*, 2012, **64**, 4248.
8 G. Soloperto, F. Conversano, A. Greco, E. Casciaro, E. Ragusa, A. Lay-Ekuakille and S. Casciaro, *IEEE Trans. Instrum. Meas.*, 2013, **63**, 1423.
9 P. Lo Meo, F. D'Anna, S. Riela, M. Gruttadauria and R. Noto, *Tetrahedron*, 2002, **58**, 6039.
10 L. Zerkoune, A. Angelova and S. Lesieur, *Nanomaterials*, 2014, **4**, 741.
11 M. Massaro, S. Riela, P. Lo Meo, R. Noto, G. Cavallaro, S. Milioto and G. Lazzara, *J. Mater. Chem. B*, 2014, **2**, 7732.
12 W. Y. Huang, Y. Z. Cai and Y. Zhang, *Nutr. Cancer*, 2010, **62**, 1.
13 B. Buhklari, S. Memon, M. M. Tahir and M. I. Bhanjer, *J. Mol. Struct.*, 2008, **892**, 39.
14 Y. Wei, X. Ye, X. Shang, X. Peng, Q. Bao, M. Liu, M. Guo and F. Li, *Colloids Surf., A*, 2012, **396**, 22.
15 Y. Zheng, I. S. Haworth, Z. Zuo, M. S. S. Chow and A. H. L. Chow, *J. Pharm. Sci.*, 2005, **94**, 1079.
16 A. Kumari, S. K. Yadav, Y. B. Pakade, B. Singh and S. C. Yadav, *Colloids Surf., B*, 2010, **80**, 184.
17 (*a*) C. Poon, C. He, D. Liu, K. Lu and W. Lin, *J. Controlled Release*, 2015, **201**, 90; (*b*) H. Wang, Y. Wu, R. Zhao and G. Nie, *Adv. Mater.*, 2013, **25**, 1616; (*c*) J. Lehar, A. S. Krueger, W. Avery, A. M. Heilbut, L. M. Johansen, E. R. Price, R. J. Rickles, G. F. Short rd, J. E. Staunton, X. Jin, M. S. Lee, G. R. Zimmermann and A. A. Borisy, *Nat. Biotechnol.*, 2009, **27**, 659.
18 P. Yuang, P. D. Southon, Z. Liu, M. E. R. Green, J. M. Hook, S. J. Antill and C. J. Kepert, *J. Phys. Chem. C*, 2008, **112**, 15742.
19 *Interfacial Phenomena Equilibrium and Dynamic Effects*, ed. C. A. Miller and P. Neogi, Marcel Dekker, Inc., New York, 1985, vol. 17.
20 G. Cavallaro, G. Lazzara and S. Milioto, *Langmuir*, 2011, **27**, 1158.
21 F. Perret, C. Marminon, W. Zeinyeh, P. Nebois, A. Bollacke, J. Jose, H. Parrot-Lopez and M. Le-Borgne, *Int. J. Pharm.*, 2013, **441**, 491.
22 C. Jullian, L. Moyano, C. Yañez and C. Olea-Azar, *Spectrochim. Acta, Part A*, 2007, **67**, 230.
23 R. De Lisi, G. Lazzara and S. Milioto, *Phys. Chem. Chem. Phys.*, 2011, **13**, 12571.
24 H. Liu, Z. Du and Q. Yuan, *J. Chromatogr. B: Anal. Technol. Biomed. Life Sci.*, 2009, **877**, 4159.
25 K. M. Tushar, S. G. Kalyan, S. Anirban and D. Swagata, *J. Photochem. Photobiol., A*, 2008, **194**, 297.
26 R. Angelico, A. Ceglie, P. Sacco, G. Colafemmina, M. Ripoli and A. Mangia, *Int. J. Pharm.*, 2014, **471**, 173.
27 X. Zhu and W. Ping, *Spectrochim. Acta, Part A*, 2014, **132**, 38.
28 I. Calabrese, G. Cavallaro, C. Scialabba, M. Licciardi, M. Merli, L. Sciascia and M. L. Turco Liveri, *Int. J. Pharm.*, 2013, **457**, 224.
29 D. A. Fulton and J. F. Stoddart, *J. Org. Chem.*, 2001, **66**, 8309.